Zr-89-labeled Bispecific T-cell Engager AMG 211 PET Shows AMG 211 Accumulation in CD3-rich Tissues and Clear, Heterogeneous Tumor Uptake

Moek, Kirsten L; Waaijer, Stijn J H; Kok, Iris C; Suurs, Frans V; Brouwers, Adrienne H; Menke-van der Houven van Oordt, Catharina W; Wind, Thijs T; Gietema, Jourik A; Schröder, Carolina P; Mahesh, Shekar V K

Published in:
Clinical Cancer Research

DOI:
10.1158/1078-0432.CCR-18-2918

Published OnlineFirst February 11, 2019; DOI: 10.1158/1078-0432.CCR-18-2918

Precision Medicine and Imaging

Clinical Cancer Research

^{89}Zr-labeled Bispecific T-cell Engager AMG 211 PET Shows AMG 211 Accumulation in CD3-rich Tissues and Clear, Heterogeneous Tumor Uptake

Kirsten L. Moek[1], Stijn J.H. Waaijer[1], Iris C. Kok[1], Frans V. Suurs[1], Adrienne H. Brouwers[2], C. Willemien Menke-van der Houven van Oordt[3], Thijs T. Wind[1], Jourik A. Gietema[1], Carolien P. Schröder[1], Shekar V.K. Mahesh[2], Annelies Jorritsma-Smit[4], Marjolijn N. Lub-de Hooge[4], Rudolf S.N. Fehrmann[1], Derk Jan A. de Groot[1], and Elisabeth G.E. de Vries[1]

Abstract

Purpose: Biodistribution of bispecific antibodies in patients is largely unknown. We therefore performed a feasibility study in 9 patients with advanced gastrointestinal adenocarcinomas to explore AMG 211 biodistribution (also known as MEDI-565), an approximately 55 kDa bispecific T-cell engager (BiTE®) directed against carcinoembryonic antigen (CEA) on tumor cells and cluster of differentiation 3 (CD3) on T-cells.

Experimental Design: ^{89}Zr-labeled AMG 211 as tracer was administered alone or with cold AMG 211, for PET imaging before and/or during AMG 211 treatment.

Results: Before AMG 211 treatment, the optimal imaging dose was 200-μg ^{89}Zr-AMG 211 + 1,800-μg cold AMG 211. At 3 hours, the highest blood pool standardized uptake value $(SUV)_{mean}$ was 4.0, and tracer serum half-life was 3.3 hours. CD3-mediated uptake was clearly observed in CD3-rich lymphoid tissues including spleen and bone marrow (SUV_{mean} 3.2 and 1.8, respectively), and the SUV_{mean} decreased more slowly than in other healthy tissues. ^{89}Zr-AMG 211 remained intact in plasma and was excreted predominantly via the kidneys in degraded forms. Of 43 visible tumor lesions, 37 were PET quantifiable, with a SUV_{max} of 4.0 [interquartile range (IQR) 2.7–4.4] at 3 hours using the optimal imaging dose. The tracer uptake differed between tumor lesions 5-fold within and 9-fold between patients. During AMG 211 treatment, tracer was present in the blood pool, whereas tumor lesions were not visualized, possibly reflecting target saturation.

Conclusions: This first-in-human study shows high, specific ^{89}Zr-AMG 211 accumulation in CD3-rich lymphoid tissues, as well as a clear, inter- and intraindividual heterogeneous tumor uptake.

Introduction

Immunotherapy with immune checkpoint inhibitors is currently used as part of many treatment regimens for a wide range of tumor types. Unfortunately, not all patients benefit from these drugs. This has stimulated the search for new drugs to induce an anticancer immune response, including bispecific antibodies (1).

One novel approach is the use of bispecific T-cell engager (BiTE) antibody constructs (a registered trade mark of Amgen Inc.). These consist of two single-chain variable fragment arms of which one is directed against an antigen target on the tumor cell membrane and the other often against cluster of differentiation 3 (CD3) on T-cells. Binding of both arms induces target cell–dependent T-cell activation and proliferation, leading to apoptosis of tumor cells (2). The anti-CD19/CD3 BiTE blinatumomab is approved for the treatment of patients with B-cell precursor acute lymphoblastic leukemia (3). Continuous intravenous administration is used because of its short serum half-life of 2 hours. This results from its small molecular size of approximately 55 kDa, which leads to renal filtration, and the lack of an Fc domain, which prevents salvation from lysosomal degradation (4, 5).

AMG 211 (also known as MEDI-565) is a carcinoembryonic antigen (CEA; CEACAM5)-directed BiTE. CEA, a glycosylated human oncofetal antigen, is abundantly expressed by a variety of tumors, especially adenocarcinomas of the gastrointestinal tract (6, 7). *In vitro* studies have shown that a low concentration of approximately 1 ng/mL of anti-CEA/CD3 AMG 211 is sufficient to activate patient-derived T-cells with subsequent lysis of patient-derived chemo-refractory CEA-positive colorectal tumor cells (8, 9).

A study in patients with advanced gastrointestinal adenocarcinomas with 0.75 μg to 7.5 mg/day AMG 211 administered intravenously over 3 hours on days 1 to 5 in 28-day cycles showed linear and dose-proportional pharmacokinetics, but no tumor responses (10). This might be related to intermittent administration and short exposure of the tumor to the drug,

[1]Department of Medical Oncology, University Medical Center Groningen, University of Groningen, Groningen, the Netherlands. [2]Department of Radiology, Nuclear Medicine and Molecular Imaging, University Medical Center Groningen, University of Groningen, Groningen, the Netherlands. [3]Department of Medical Oncology, VU University Medical Center, Amsterdam, the Netherlands. [4]Department of Clinical Pharmacy and Pharmacology, University Medical Center Groningen, University of Groningen, Groningen, the Netherlands.

Note: Supplementary data for this article are available at Clinical Cancer Research Online (http://clincancerres.aacrjournals.org/).

Corresponding Author: Elisabeth G.E. de Vries, University of Groningen, University Medical Center Groningen, P.O. Box 30.001, Groningen 9700 RB, the Netherlands. Phone: 315-0361-2934; Fax: 315-0361-4862; E-mail: e.g.e.de.vries@umcg.nl.

Clin Cancer Res 2019;25:3517–27

doi: 10.1158/1078-0432.CCR-18-2918

Published OnlineFirst February 11, 2019; DOI: 10.1158/1078-0432.CCR-18-2918

Translational Relevance

Bispecific antibodies, including approximately 55 kDa bispecific T-cell engager (BiTE) antibody constructs, can be used to induce an anticancer immune response. Although CD19/CD3-directed BiTE blinatumomab already received FDA approval, several other bispecific antibodies are in various stages of clinical development. Little is known about biodistribution of these drugs in patients. With bispecific antibodies, the potentially different binding affinities for the target of each of the arms might affect biodistribution, as has already been shown in preclinical models. Knowledge about biodistribution might be helpful regarding drug dosing schedules and can support rational trial design. In this study, we demonstrated that imaging with ^{89}Zr-AMG 211 is very informative regarding CEA/CD3 BiTE antibody construct, whole-body biodistribution, and tumor targeting. We showed cluster of differentiation 3 (CD3)-specific tracer accumulation in lymphoid organs and clear tumor uptake that was highly heterogeneous, both within and between patients.

which has an elimination half-life of 2.2 to 6.5 hour. To achieve sustained target coverage, thereafter AMG 211 was administered and tested as a continuous intravenous infusion for 28 subsequent days in 6-week treatment cycles in a phase I study in patients with advanced gastrointestinal adenocarcinomas (11).

In bispecific antibodies, the potentially different binding affinity for the target of each of the arms might affect biodistribution. However, very limited information is available regarding whole-body distribution of bispecific antibodies and BiTE antibody constructs in patients (12, 13). Improved understanding of biodistribution of these bispecific antibody constructs might help to guide drug dosing schedules and inform potential target-related drug impact *in vivo*. PET with zirconium-89 (^{89}Zr)-labeled AMG 211 as a tracer has shown specific tracer uptake in human CEA-expressing tumor-bearing mice (14). Therefore, we performed a first-in-human feasibility study with the ^{89}Zr-labeled BiTE antibody construct AMG 211 and PET imaging to determine the biodistribution of ^{89}Zr-AMG 211 in healthy tissues and tumor lesions before and/or during AMG 211 treatment in the AMG 211 phase I study.

Materials and Methods

Patients

Patients with pathologically proven gastrointestinal adenocarcinomas were eligible for this imaging study (ClinicalTrials.gov identifier NCT02760199) if they were participating in the phase I study with AMG 211 (ClinicalTrials.gov identifier NCT02291614) at the University Medical Center Groningen (UMCG; Groningen, the Netherlands) or the Free University Medical Center (VUMC; Amsterdam, the Netherlands). Other eligibility criteria included age $\geq$18 years, written informed consent, and availability of $\geq$1 measurable lesion as assessed with CT per modified immune-related response criteria (irRC; ref. 15). For visceral lesions, this is defined as the two longest perpendicular diameters $\geq 10 \times 10$ mm, and for pathologic lymph nodes as the longest diameter perpendicular to the longest axis $\geq$15 mm.

This study was conducted in compliance with the Declaration of Helsinki, ICH harmonized Tripartite Guideline for Good Clinical Practice (ICH-GCP) and applicable national and local regulatory requirements. This study was centrally approved by the Medical Ethical Committee of the UMCG and the Central Committee on Research Involving Human Subjects, the competent authority in the Netherlands. All patients provided written informed consent.

Study design

This two-center imaging study was performed at the UMCG and the VUMC, both university medical centers in the Netherlands. In the phase I study, patients received continuous intravenous treatment with 6,400-µg/day or 12,800-µg/day AMG 211 via a central venous access port for 28 subsequent days ("treatment period") in 42-day cycles. The imaging study was performed before AMG 211 treatment and/or immediately after the end of the second AMG 211 treatment period of 28 days ("during AMG 211 treatment") as is illustrated in Fig. 1.

The tracer ^{89}Zr-AMG 211 was produced in the UMCG under good manufacturing practice conditions, as described previously (14, 16). Briefly, AMG 211, which was produced and provided by MedImmune via collaboration with Amgen, was reacted with a 4-fold molar excess of the tetrafluorphenol-N-succinyldesferal-Fe ester (N-Suc-Df; ABX) and purified by gel filtration using PD-10 columns. The conjugate N-SucDf-AMG 211 was radiolabeled with clinical grade ^{89}Zr-oxalate (PerkinElmer) and again purified by gel filtration. Individual fractions were pooled on the basis of the amount of radioactivity and radiochemical purity. Quality control of intermediate and final drug product consisted of determination of conjugation ratio, aggregation, radiochemical purity, and stability. Immunoreactivity tests on the extracellular domain of CEA showed that ^{89}Zr-AMG 211 was still capable of specific binding to its target. In addition, a binding assay on $CD3^+$ T-cells was performed to confirm binding of N-SucDf-AMG 211 to CD3.

In 8 patients, ^{89}Zr-AMG 211 imaging was performed before AMG 211 treatment. These patients received, via a separate intravenous line, a fixed dose of 37 MBq approximately 200-µg ^{89}Zr-AMG 211 alone ($n = 2$), or in combination with 1,800-µg ($n = 4$) or 4,800-µg ($n = 2$) cold AMG 211, administered in 3 hours. This 3-hour period was based on the MTD and infusion rate as assessed in the phase I study. Cold AMG 211 was added to guarantee sufficient tracer availability and was therefore administered before ^{89}Zr-AMG 211 (details in Supplementary Materials and Methods: ^{89}Zr-AMG 211 administration). We considered the cold AMG 211 dose to be sufficient when the circulation could be adequately visualized at each PET scan time point as used in other studies with comparable design. To mitigate AMG 211-related cytokine release syndrome, 4-mg dexamethasone was administered orally 1 hour before the cold AMG 211 infusion, and at 3 hours and 6 hours thereafter. AMG 211 treatment started 7 days after tracer injection. Moreover, in 2 patients, 200-µg ^{89}Zr-AMG 211 was administered over 3 hours via a separate intravenous line to study biodistribution immediately after the end of the second AMG 211 treatment period. In one of these 2 patients, PET imaging was also performed before AMG 211 treatment. After tracer infusion, patients were observed in the hospital for 24 hours to detect any side effects. The NCI Common Terminology Criteria for Adverse Events (NCI CTCAE) v4.03 were used for grading of adverse events (17).

Published OnlineFirst February 11, 2019; DOI: 10.1158/1078-0432.CCR-18-2918

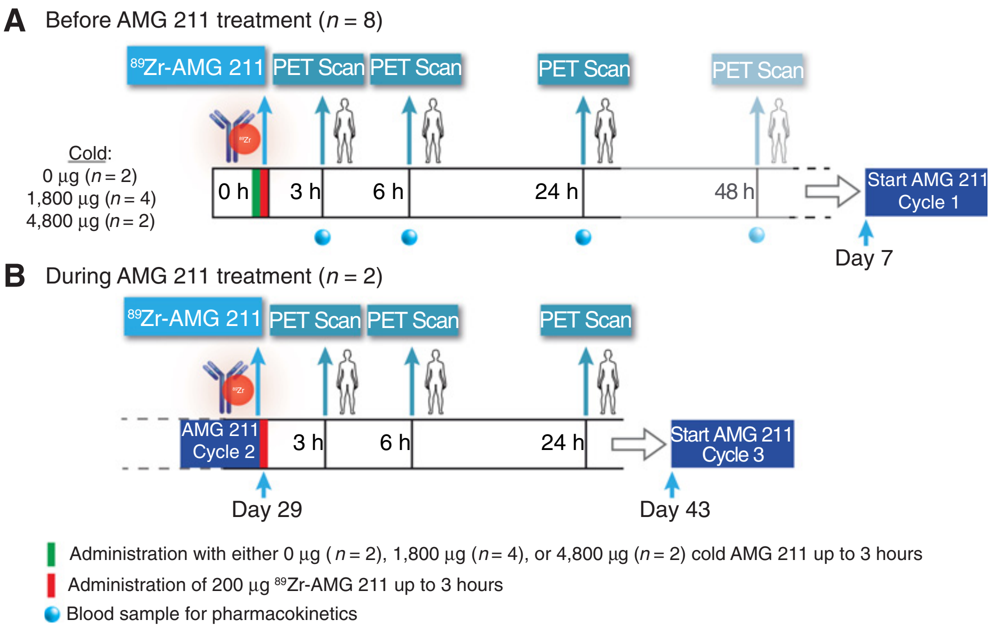

Figure 1.

Study design of ^{89}Zr-AMG 211 PET imaging before (**A**) and during (**B**) AMG 211 treatment. The PET scan at 48 hours is shown vaguely, because this time point was changed into 3 hours after imaging was performed in the first patient.

PET/CT scans were performed from the top of the skull to mid-thigh with a 40-slice or 64-slice PET/CT camera (Biograph mCT, Siemens in the UMCG and Gemini TF or Ingenuity TF, Philips in the VUMC) initially 6, 24, and 48 hours after completion of the tracer injection. This was changed into 3, 6, and 24 hours from the second patient onwards, based on a review of data from the first patient showing rapid ^{89}Zr-AMG 211 clearance from the circulation [blood pool standardized uptake value (SUV)$_{mean}$ 0.2 at 24 hours]. For attenuation correction and anatomic reference, a low-dose CT scan was acquired immediately before the PET scan.

Diagnostic CT scans of the chest and abdomen were performed within 21 days before ^{89}Zr-AMG 211 injection and for response evaluation after every two AMG 211 treatment cycles.

^{89}Zr-AMG 211 PET analysis

All PET scans were reconstructed using the harmonized reconstruction algorithm recommended for multicenter ^{89}Zr PET scan trials (18). A single nuclear medicine physician analyzed all the PET scans for visible tracer uptake in tumor lesions and healthy tissues including lymph nodes. The total number and location of measurable tumor lesions, according to irRC, were assessed with diagnostic CT. Tumor lesions with visible tracer uptake on the ^{89}Zr-AMG 211 PET were considered quantifiable when the tumor size was at least 15 mm on CT to minimize potential partial volume effect. Radioactivity was quantified by manually drawing spherical volumes of interest (VOI) in healthy tissues and tumor lesions using A Medical Image Data Examiner (AMIDE) software (version 0.9.3, Stanford University, Stanford, CA; ref. 19). In healthy tissues, VOIs were drawn in the blood pool at the place of the thoracic aorta, lung, liver, spleen, kidney, intestine, brain, bone marrow, and bone cortex at the place of the femur, thigh muscle, retroperitoneum, and fat tissue. VOIs were drawn independently by two investigators, K.L. Moek and I.C. Kok, based on maximum intensity projection images of ^{89}Zr-AMG 211 PET or the coregistered low-dose CT if delineation was unclear on PET. ^{89}Zr-AMG 211 uptake was measured as SUV (formula in Supplementary Materials and Methods: calculations). We reported SUV$_{max}$ (maximum voxel intensity in the VOI) for tumor lesions and SUV$_{mean}$ (mean voxel intensity of all voxels in the VOI) for healthy tissues. Outliers were reassessed for accuracy. In case of a discrepancy $\geq$10% between the two investigators, the discrepancies were discussed and a final conclusion made. In addition, the percentage injected dose per kilogram (%ID/kg) was calculated for all VOIs (formula in Supplementary Materials and Methods: calculations). For the brain, lungs, liver, spleen, and kidneys, we used mean organ weights as reported in sudden death autopsy studies to calculate percentage of the injected dose (%ID; refs. 20, 21). We used the percentage body fat and total bodyweight to assess %ID in fat (22). The total blood volume was calculated according to Nadler's formula (23) and ^{89}Zr-AMG 211 serum half-life with a 1-phase decay model using GraphPad Prism software version 5.04.

Pharmacokinetic assessments of ^{89}Zr in blood and urine samples

To study ^{89}Zr pharmacokinetics, blood and urine samples were collected at each PET scan time point. In addition, ^{89}Zr-AMG 211 binding to immune cells was explored by counting blood fractions, and the integrity was analyzed via gel electrophoresis. More details on ^{89}Zr pharmacokinetics are provided in Supplementary Materials and Methods: ^{89}Zr pharmacokinetics.

Soluble CEA, antidrug antibodies, and tumor CEA expression

Blood samples for soluble CEA were collected at screening and after the second AMG 211 treatment cycle. Serum soluble CEA upper limit of normal was 5 µg/L. In addition, serum antidrug antibody (ADA) levels were determined in blood samples, collected day 1 before and 7 days after tracer infusion, with an

Published OnlineFirst February 11, 2019; DOI: 10.1158/1078-0432.CCR-18-2918

electrochemiluminescent assay for patients imaged during AMG 211 treatment. Tumor CEA expression was verified in archival tumor tissues. CEA membranous and cytoplasmic staining was scored as 3+ for strong, 2+ for moderate, 1+ for weak, and 0 for absence of any staining. A tumor was considered to express the CEA protein if at least 2+ protein expression was seen.

Statistical analysis

Statistical analyses were performed using SPSS Version 23. Unless stated otherwise, data are shown as median with interquartile range (IQR) or range in case $n \leq 3$. Associations between parameters were calculated using the Spearman correlation test. *P* values < 0.05 were considered significant.

Results

Patient characteristics

Nine patients were enrolled between August 2016 and May 2017. The ^{89}Zr-AMG 211 PET imaging study was terminated in May 2017 because of the completion of the AMG 211 phase I study. ^{89}Zr-AMG 211 PET imaging was performed in 7 patients before treatment with 6,400-µg/day AMG 211, in one patient during treatment with 12,800-µg/day AMG 211, and in one patient PET imaging was performed before as well as during treatment with 6,400-µg/day AMG 211. This makes the total number of PET series studied 10. Patient characteristics are shown in Table 1. CEA tumor expression was positive in all 7 patients, from whom archival tumor tissue was available.

^{89}Zr-AMG 211 healthy tissue biodistribution before AMG 211 treatment

Median radioactivity dose administered across all patients was 35.77 MBq (IQR 34.90–36.99 MBq). Because of technical reasons, one 6-hour PET scan of one patient receiving 200-µg ^{89}Zr-AMG 211 + 1,800-µg cold AMG 211 was not evaluable.

With 200-µg ^{89}Zr-AMG 211 ($n = 2$), SUV$_{mean}$ in the blood pool at 3 hours was 2.2, which decreased thereafter (Fig. 2A and B). The addition of 1,800-µg cold AMG 211 ($n = 4$) resulted in a higher blood pool SUV$_{mean}$ of 4.0 (IQR 3.2–5.6) at 3 hours. The addition of 4,800-µg cold AMG 211 ($n = 2$) did not further increase blood pool SUV$_{mean}$ at any time point. We, therefore, determined that 200-µg ^{89}Zr-AMG 211 + 1,800-µg cold AMG 211 was optimal for ^{89}Zr-AMG 211 PET imaging before AMG 211 treatment. The corresponding ^{89}Zr-AMG 211 serum half-life was 3.3 hours (Supplementary Table S1), indicating the optimal time points for ^{89}Zr-AMG 211 PET imaging period to be around 3, and 6 hours after tracer administration. Figure 2D illustrates whole-body maximum intensity projection PET images for all time points of one patient in whom imaging was performed before AMG 211 treatment using 200-µg ^{89}Zr-AMG 211 + 1,800-µg cold AMG 211.

Healthy tissue biodistribution in the 4 patients who received 200-µg ^{89}Zr-AMG 211 + 1,800-µg cold AMG 211 showed high (Fig. 2A) and prolonged (Fig. 3) tracer uptake in the CD3-rich tissues in spleen and bone marrow. Liver uptake at 3 hours showed a SUV$_{mean}$ of 3.1 (IQR 2.4–3.5). AMG 211 was at that time already clearly being excreted by the kidneys. Much lower uptake at 3 hours was observed in lung, bone, muscle, abdominal cavity, brain, and body fat (Fig. 2A). In all healthy tissues analyzed, SUV$_{mean}$ was highest at 3 hours and decreased over time, except for the intestines, in which the SUV$_{mean}$ increased from 1.9 (IQR 1.5– 2.3) at 3 hours, to 2.5 (IQR 1.7–3.9) at 24 hours. Accumulation of ^{89}Zr-AMG 211 was visually observed in the colon, but not in other parts of the gastrointestinal (GI) tract known to physiologically overexpress CEA, like the stomach or esophagus (7). Healthy tissue biodistribution at 3 hours for all imaging dosing cohorts is shown in Fig. 2A. Supplementary Table S2 shows median ^{89}Zr-AMG 211 uptake in kidneys, liver, spleen, bone marrow, lung, and intestine across all imaging dosing cohorts per PET scan time point.

In patients receiving 200-µg ^{89}Zr-AMG 211 + 1,800-µg cold AMG 211, at 3 hours 26.1 %ID was present in the blood pool, 0.4 %ID in the spleen, 6.1 %ID in the liver, 32.7 %ID in the kidneys, and 3.6 %ID in the total fatty tissue. The %ID at 3 hours across all imaging dosing cohorts is shown in Supplementary Fig. S1.

^{89}Zr-AMG 211 uptake in tumor lesions before AMG 211 treatment

A total of 61 tumor lesions $\geq 10 \times 10$ mm (median per patient: 8, range 2–14) were identified on the basis of a diagnostic CT scan (Supplementary Table S3). Of these lesions, 62% ($n = 38$) could be visualized on PET. In addition, visual tracer presence was observed in four presumably malignant lymph nodes <10 mm, and one lesion in the sacral bone, which was positioned outside the view of the diagnostic CT scan. Fourteen lesions were visible as "hot spots", whereas liver ($n = 27$) and renal ($n = 2$) metastases appeared visually as "cold spots" due to the relatively high uptake in the surrounding healthy tissue. Of the 43 visible tumor lesions, 37 (86%) were PET-quantifiable (Supplementary Table S3). Two renal lesions were considered not quantifiable due to the extremely high uptake in the surrounding healthy kidney tissue, whereas four lymph nodes suspected to be malignant were not quantifiable due to the small size of these structures, which impeded quantification.

Table 1. Patient characteristics at baseline

Characteristics	
Age, median years (range)	64 (51–79)
Sex	
Male, *n*	7
Female, *n*	2
Body weight, median in kg (range)	79 (61–120)
Karnofsky performance status, *n*	
100%	1
90%	3
80%	5
Tumor type, *n*	
Appendix adenocarcinoma	1
Colorectal adenocarcinoma	6
Pancreatic adenocarcinoma	2
Tumor lesions $\geq 10 \times 10$ mm, median *n* (range)	6 (2–15)
Prior systemic noncurative therapies, *n*	
1	1
2	3
3	5
AMG 211 treatment dose, *n*	
6,400-µg/day for 28 days	8
12,800-µg/day for 28 days	1
Soluble serum CEA, in µg/L	
Appendix adenocarcinoma	2
Colorectal adenocarcinoma, median (range)	130 (6–320)
Pancreatic adenocarcinoma	11, 21
IHC CEA expression on archival tumor tissue, *n*	
Positive	7
Negative	0

Published OnlineFirst February 11, 2019; DOI: 10.1158/1078-0432.CCR-18-2918

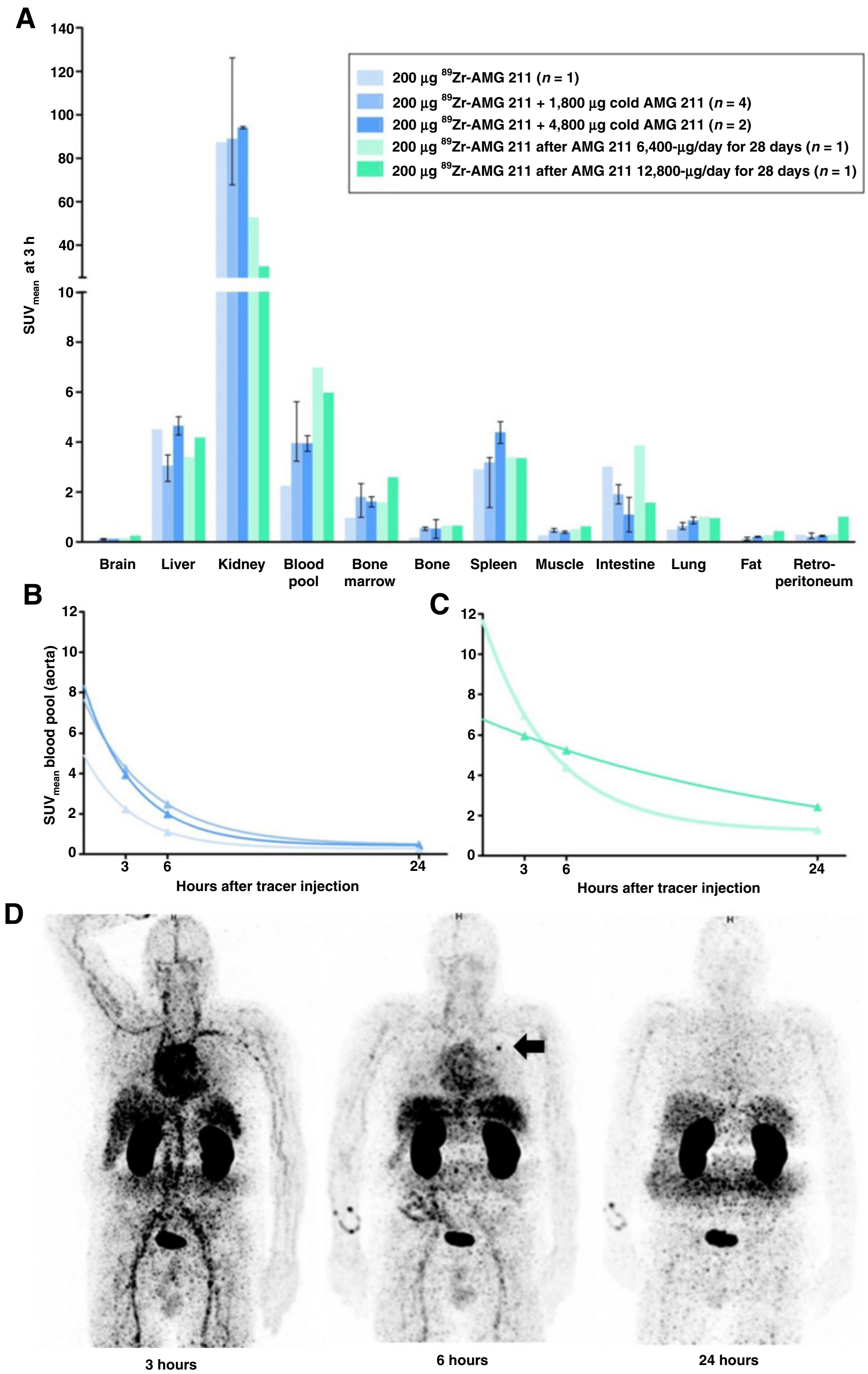

Figure 2.
^{89}Zr-AMG 211 healthy tissue biodistribution. **A,** ^{89}Zr-AMG 211 healthy tissue biodistribution 3 hours post tracer administration for the different dosing cohorts used for imaging before (blue) and during (green) AMG 211 treatment. Data shown as median SUV$_{mean}$, error bars. **B,** Nonlinear regression curve showing mean SUV$_{mean}$ in the blood pool measured in the thoracic aorta per PET scan time point before AMG 211 treatment, and during AMG 211 treatment (**C**). **D,** ^{89}Zr-AMG 211 maximum intensity projection images of one patient imaged with 200-µg ^{89}Zr-AMG 211 and 1,800-µg cold AMG 211 showing a rapidly decreasing uptake in heart and blood pool over time. Healthy tissue biodistribution showed very high tracer presence in the kidneys and bladder, and high uptake in liver and spleen across all PET scan time points. The PET scan performed 6 hours post tracer injection showed high uptake in a tumor lesion localized in the upper lobe of the left lung (arrow). H, hours.

In the imaging dosing cohort given 200-µg ^{89}Zr-AMG 211 + 1,800-µg cold AMG 211, a SUV$_{max}$ of 4.0 (IQR 2.7–4.4) at 3 hours was found in tumor lesions, decreasing to 2.8 (IQR 2.0–3.3) at 24 hours. A patient-based analysis showed a slower tumor ^{89}Zr-AMG 211 washout than from the blood pool and from most healthy tissues, except for the spleen, bone marrow, and intestines, indicating tracer specificity (Fig. 3). Figure 4 is a heat map with log ratios for SUV across tumor lesions and healthy tissues for this imaging dosing cohort, showing that the maximum voxel intensity in tumor lesions exceeds the mean voxel intensity in healthy

Published OnlineFirst February 11, 2019; DOI: 10.1158/1078-0432.CCR-18-2918

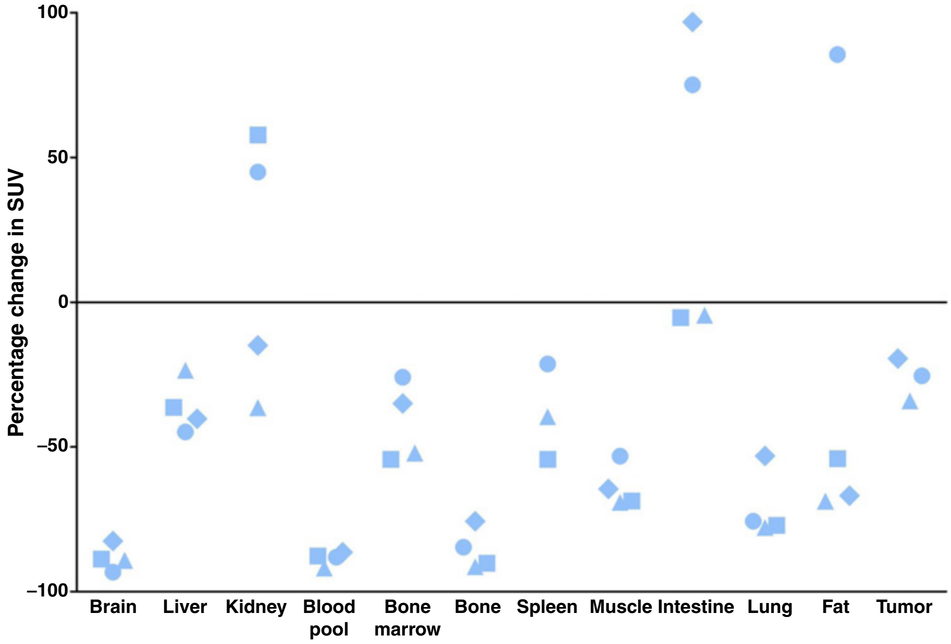

Figure 3.
Percentage change of tracer uptake between the 3 hours and 24 hours PET scan time points. Data is shown for 4 patients who received 200-µg ^{89}Zr-AMG 211 + 1,800-µg cold AMG 211 before AMG 211 treatment. Each individual patient is represented by either a square, circle, triangle, or diamond.

tissues, except for the kidneys. In the other imaging dosing cohorts, at 3 hours, a tumor lesion SUV_{max} of 2.9 (IQR 2.3–4.4) was found in the 200-µg ^{89}Zr-AMG 211 cohort, and a tumor lesion SUV_{max} of 3.1 (IQR 2.7–5.3) was found in the 200-µg ^{89}Zr-AMG 211 + 4,800-µg cold AMG 211 cohort. These findings also confirm that 200-µg ^{89}Zr-AMG 211 + 1,800-µg cold AMG 211 is optimal for imaging.

In all imaging dosing cohorts, ^{89}Zr-AMG 211 tumor uptake varied greatly within and between patients. To study this heterogeneity in tumor lesion uptake, we used the 6-hour PET scan with higher tumor-to-blood ratios than the 3-hour scan. Lesion-based analysis showed up to a 9-fold difference in ^{89}Zr-AMG 211 tumor lesion uptake between patients, irrespective of tumor localization (Fig. 5). Moreover, Fig. 5 illustrates representative PET/CT scans from a patient showing highly heterogeneous ^{89}Zr-AMG 211 uptake across lung metastases. Patient-based analysis showed a 5-fold difference in tumor lesion tracer uptake within one organ.

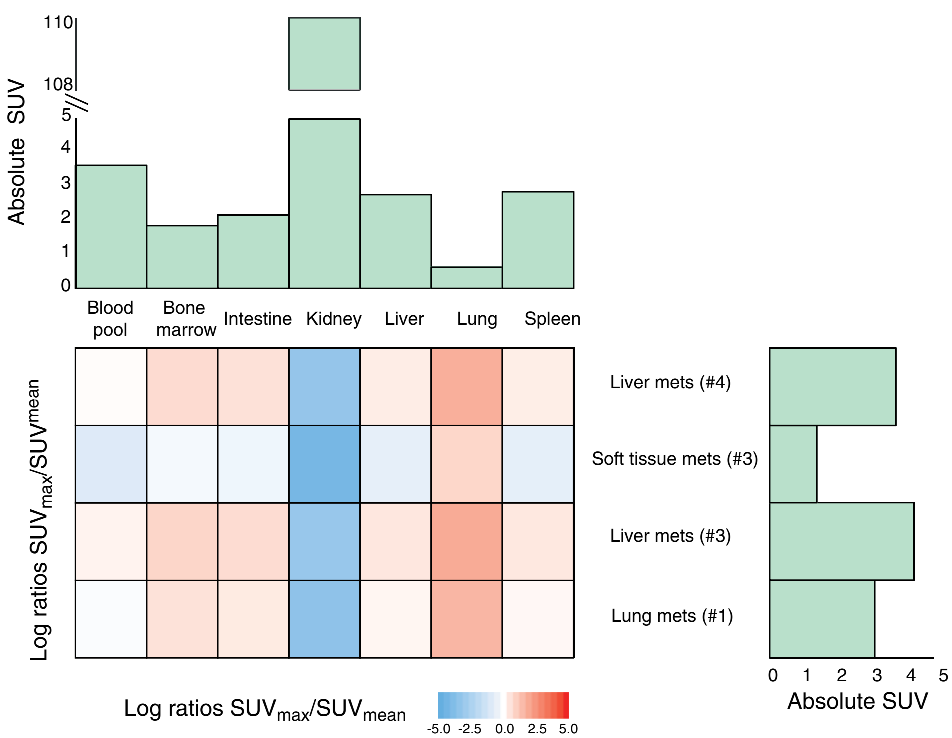

Figure 4.
Heat map and absolute uptake of healthy tissues and tumor lesions. The heat map shows log ratios obtained by dividing the ^{89}Zr-AMG 211 uptake expressed in SUV_{max} in tumor lesions by the uptake expressed in SUV_{mean} in healthy tissues across patients in whom imaging was performed before AMG 211 treatment using 200-µg ^{89}Zr-AMG 211 and 1,800-µg cold AMG 211. Quantification of ^{89}Zr-AMG 211 uptake across healthy tissues and tumor lesions is shown in the histograms. Data is based on ^{89}Zr-AMG 211 SUVs at 3 hours in visible tumor lesions (liver, soft tissue, and lung) across $n = 3$ patients and healthy tissue (blood pool, bone marrow, intestine, kidney, liver, lung, and spleen) across $n = 4$ patients. Tumor lesions of one patient were not PET quantifiable. Mets, metastases.

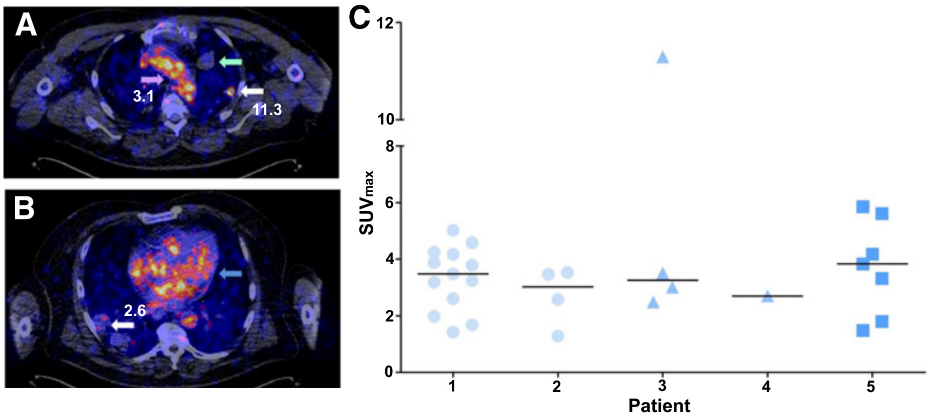

Figure 5.

Heterogeneous tumor uptake illustrated by ^{89}Zr-AMG 211 PET imaging. **A,** Patient with lung metastases of colon cancer imaged 6 hours post tracer injection with 37 MBq 200-µg ^{89}Zr-AMG 211 + 1,800-µg cold AMG 211. Transverse plane of fused PET/CT (low-dose CT) of the chest showing high tracer presence in aortic arch (pink arrow) and high uptake in a lung metastasis with a SUV_{max} of 11.3 (white arrow), whereas another lung metastasis did not show visual tracer uptake (green arrow), and high tracer presence in the heart (**B**; blue arrow) and uptake in a lung metastasis with a SUV_{max} of 2.6 (white arrow). **C,** Heterogeneous ^{89}Zr-AMG 211 uptake in tumor lesions within and in between patients on PET imaging before AMG 211 treatment. Uptake expressed in SUV_{max} (on *y*-axis) at 6 hours post tracer administration, bars display median tumor uptake. Each imaging dosing cohort is represented by a symbol: circle, 200-µg ^{89}Zr-AMG 211; triangle, 200-µg ^{89}Zr-AMG 211 + 1,800-µg cold AMG 211; and square, 200-µg ^{89}Zr-AMG 211 + 4,800-µg cold AMG 211.

Analysis of relation between tumor uptake and tumor response to AMG 211 treatment was not possible, as response evaluation after the second AMG 211 treatment cycle could only be performed in 2 patients. In the other patients, treatment was stopped prematurely due to either rapid clinical progressive disease ($n = 4$) or adverse events ($n = 1$), and one patient did not start with AMG 211 treatment due to clinical deterioration caused by tumor progression.

^{89}Zr-AMG 211 healthy tissue biodistribution and uptake in tumor lesions during AMG 211 treatment

^{89}Zr-AMG 211 imaging immediately after the end of the second AMG 211 treatment period was performed in 2 patients who received 28-day continuous intravenous treatment with either 6,400-µg/day or 12,800-µg/day of AMG 211 per cycle. Because of completion of the phase I treatment part of the study, no additional patients were enrolled in this imaging dosing cohort.

During AMG 211 treatment, we observed an approximately 2–3-fold higher uptake in the blood pool and an approximately 2–3-fold lower uptake in the kidneys when compared with imaging before AMG 211 treatment (Fig. 2A and C). ^{89}Zr-AMG 211 serum half-life exceeded 16 hours in one patient (Supplementary Table S1). Seven tumor lesions with a size $\geq 10 \times 10$ mm were detected with diagnostic CT. None of these lesions, all located outside the liver and kidneys, visually showed ^{89}Zr-AMG 211 uptake. No lesions were identified on PET that were not visible on diagnostic CT.

Blood and urine pharmacokinetics

Whole-blood and urine samples for ^{89}Zr-AMG 211 measurements were available for 8 patients who underwent imaging before AMG 211 treatment. The SUV equivalents of *ex vivo* measurements of blood samples at 3, 6, 24, and 48 hours correlated well with PET-derived SUV_{mean} blood pool values (Spearman correlation coefficient = 0.983, $P \leq 0.01$). In urine, uptake at 3 hours ranged from 13.7 in $n = 1$ patient receiving 200-µg ^{89}Zr-AMG 211 to 35.1 in $n = 2$ patients receiving 200-µg ^{89}Zr-AMG 211 + 4,800-µg AMG 211. In the 200-µg ^{89}Zr-AMG 211 + 1,800-µg AMG 211 cohort, the highest radioactivity (28.7 at 3 hours) was measured in urine of one diabetic patient with proteinuria.

A median of 96.07% (IQR 95.84–96.19) of ^{89}Zr-AMG 211 was unbound in plasma, and 2.56 % (IQR 2.07–3.07) was bound to buffy coat at 3 hours. ^{89}Zr-AMG 211 was intact in plasma, whereas in urine, ^{89}Zr-AMG 211 was mostly present in degraded form (Fig. 6).

Soluble CEA and determination of ADAs

Two patients had high serum soluble CEA levels at screening, whereas the levels in the other patients ranged between 2.4 and 42.8 µg/L. In one patient who received 200-µg ^{89}Zr-AMG 211, the CEA level was 217 µg/L, whereas in the other patient who received 200-µg ^{89}Zr-AMG 211 + 1,800-µg cold AMG 211, this level was 320 µg/L. In both patients, imaging was performed before AMG 211 treatment and showed, in comparison with patients from the same imaging dosing cohort, the highest tracer presence in the blood pool.

No induction of ADAs by tracer dose was observed in patients in whom imaging was performed before AMG 211 treatment. When imaging was performed during AMG 211 treatment, ADAs were measured in serum 1 week after tracer administration in both patients.

Adverse events

No ^{89}Zr-AMG 211-related toxicity was seen, apart from known adverse events of AMG 211 itself. Two patients, one participating in the 200-µg ^{89}Zr-AMG 211 imaging dosing cohort and the other in the 200-µg ^{89}Zr-AMG 211 + 4,800-µg cold AMG 211 imaging dosing cohort, experienced fever and/or chills. The first patient also experienced headache. All adverse events occurred within 24 hours after tracer administration and are most likely due to

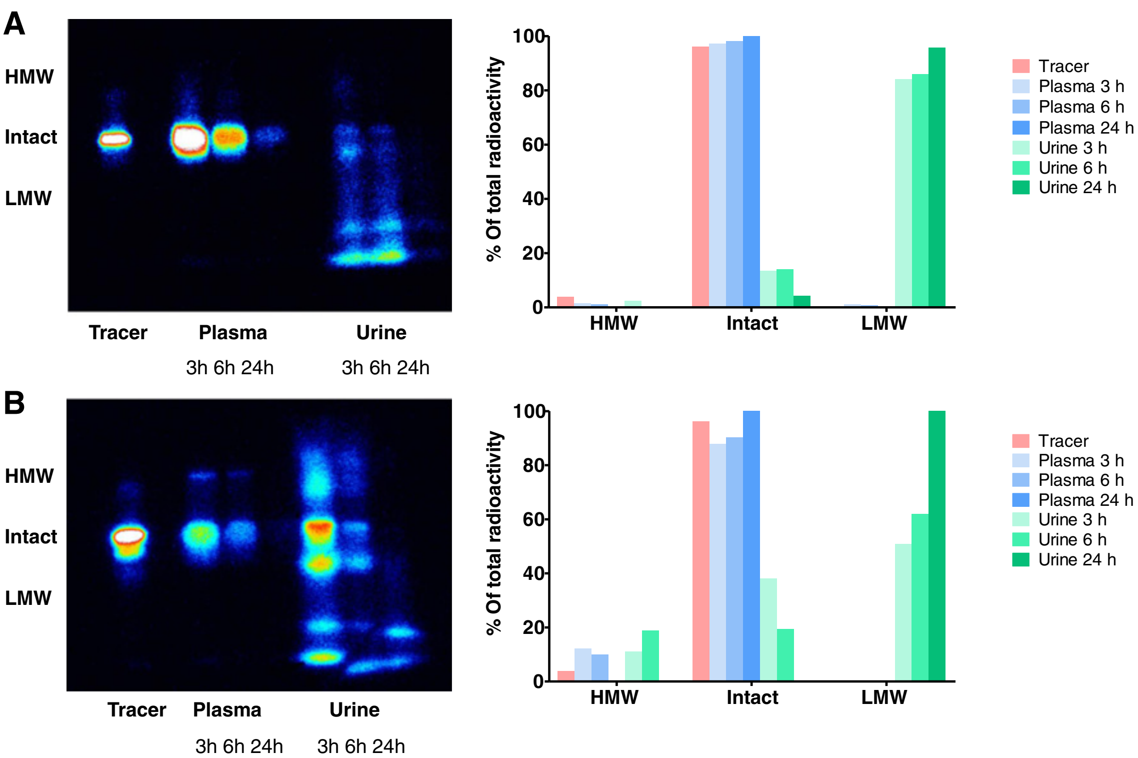

Figure 6.
^{89}Zr-AMG 211 integrity analysis. Tracer integrity analysis in one nondiabetic patient (**A**), and one diabetic patient (**B**) known to have microscopic diabetic proteinuria showing intact ^{89}Zr-AMG 211 at plasma for 24 hours and degraded ^{89}Zr-AMG 211 in urine. In the diabetic patient, high molecular weight protein was found in urine. H, hours; HMW, high molecular weight; LMW, low molecular weight.

cytokine release. Adverse events were CTCAE grade 1, and resolved spontaneously or after administration of acetaminophen.

Discussion

This is the first-in-human PET imaging study with a small BiTE antibody construct. With ^{89}Zr-labeled AMG 211-targeting CEA/CD3, high specific tracer accumulation was observed in CD3-rich lymphoid tissues such as the spleen and bone marrow and in tumor lesions. ^{89}Zr-AMG 211 was rapidly cleared from the blood pool by excretion via the kidneys, whereas uptake in tumor lesions persisted. Tumor lesions showed a clear but heterogeneous uptake within and between patients with gastrointestinal adenocarcinomas.

To date, more than one hundred bispecific antibodies have been developed, including BiTE antibody constructs, dual-affinity retargeting antibodies, and full-length antibodies (1, 24). It is well acknowledged that their development for clinical use has been more challenging for this "high hanging fruit" compared with conventional mAbs (1). The two arms differ in binding affinity for targets, which consequently might affect tissue distribution and accumulation *in vivo*. In human CD3-expressing transgenic immunocompetent mice bearing a murine tumor transfected with human HER2, the distribution of a HER2-CD3 full-length bispecific antibody was predominantly determined by the CD3 arm (25). This is because high affinity for CD3 reduced the systemic exposure and shifted antibody distribution away from tumors to T-cell containing tissues (25). Moreover, side effects in cynomolgus monkeys were dependent on the affinity of the CD3 part of a full-length CLL-1-CD3 bispecific antibody, with the high-affinity variant being poorly tolerated because of extensive cytokine release (26). In mice cografted with CEA-expressing tumor cells injected into the flank, and human peripheral blood mononuclear cells, fluorescence imaging with a CEA-CD3 full-length bispecific antibody showed tumor-specific accumulation mainly through CEA binding, with only minor contributions from CD3 binding (27). This antibody has a monovalent low affinity for CD3, in comparison with a higher bivalent affinity for CEA. With respect to AMG 211, binding affinity is also higher for CEA than for CD3, with an equilibrium dissociation constant of 5.5 nmol/L for CEA and 310 nmol/L for CD3 (28). Despite the lower affinity for CD3, we observed high ^{89}Zr-AMG 211 uptake in the spleen, and bone marrow. Because the CD3 protein complex is a defining feature of the T-cell lineage, uptake in lymphoid tissues known to be T-cell reservoirs indicate tracer specificity (29). The ^{89}Zr-AMG 211 accumulation we observed in the spleen and bone marrow likely represents the CD3-mediated uptake. However, this finding should be interpreted with some caution, because for some patients, uptake in spleen and bone marrow was lower than observed in the blood pool. This could indicate that to some extent, tracer uptake is nonspecific, or tissue target saturation was reached. In the GI tract, visual tracer accumulation was limited to the intestines, which may reflect tracer excretion in the gut and feces as well as CEA- and CD3-mediated tracer uptake in gut tissue.

Published OnlineFirst February 11, 2019; DOI: 10.1158/1078-0432.CCR-18-2918

Uptake increased over time up to the 24-hour time point, indicating that more time is needed for tracer penetration into GI tissues than into organs with a rich blood supply like kidneys and liver.

We clearly observed uptake in tumor lesions that persisted longer than tracer presence in the blood. These SUVs were higher than expected on the basis of preclinical data in mice-bearing CEA-expressing LS174T human colorectal adenocarcinoma xenografts (14). Moreover, in the clinical setting the CD3 arm can be studied, which is not possible in the preclinical mouse–mouse environment because AMG 211 is not cross-reactive with mouse CD3. Noninvasive whole-body PET imaging studies used to investigate the biodistribution of other drugs have shown considerable heterogeneity regarding tracer uptake in tumor lesions (30–32). We also observed striking intra- and interpatient heterogeneity in ^{89}Zr-AMG 211 tumor accumulation before AMG 211 treatment. This might reflect the fact that tracer accumulation is dependent on target expression as well as delivery by tumor vasculature, and tissue permeability (33). IHC target staining of multiple tumor lesions within one patient might have shed light on these differences with regards to the role of target expression. However, multiple biopsies were not part of this trial. Data on heterogeneity was lacking in the small studies, which reported tumor uptake of full-length bispecific antibodies (12, 13). In 1996, the first attempts to radiolabel bispecific antibody OC/TR F(ab')2 (folate-binding protein-CD3) were made in a small single-photon emission CT study in patients suspected to have ovarian cancer. The tumor could be visualized in 2 of 3 patients, but the study was stopped prematurely because of unexpected severe tracer-related toxicity due to cytokine release at doses as low as 0.1 mg (12). More recently, a preliminary report described ^{89}Zr-labeled cergutuzumab amunaleukin (CEA-IL2v) PET in 23 patients with solid tumors, showing CEA-mediated accumulation in tumors and uptake in lymph nodes and spleen (13). Uptake in these lymphoid organs, 5 days after tracer administration, was higher than observed in our study, likely due to the relatively long half-life of full-length antibodies, enabling prolonged tracer exposure.

Our bispecific antibody construct is small (55 kDa), resulting in a short tracer half-life as determined via a 1-phase decay model. Fast serum tracer clearance was also found in PET studies with other small-sized antibody-related radiolabeled approximately 100 kDa F(ab')$_2$ fragments of trastuzumab or approximately 15 kDa nanobodies developed as diagnostics patients with in breast cancer (34–36). These kinetics, therefore, require imaging assessments at earlier time points in comparison with approximately 150 kDa mAbs, for which scans are generally performed 4 to 7 days after tracer administration, thus matching the half-life of these compounds (30–32, 37). The small size of a BiTE antibody construct leads to fast renal clearance (38). For this reason, the drug was administered as continuous intravenous infusion (11). Interestingly, currently BiTE antibody constructs are being developed, which contain an Fc-domain (39, 40). This increases their size and leads to an enhanced serum half-life. In nonhuman primates, the serum half-life of various BiTE antibody constructs was extended from 6 to 44–167 hours by the addition of an Fc-domain or albumin (39). These larger BiTE antibody constructs exceed the renal filtration threshold of 60 kDa.

In our study, AMG 211 treatment clearly altered ^{89}Zr-AMG 211 biodistribution, leading to high and sustained ^{89}Zr-AMG 211 presence in the blood pool, which could reflect tissue target saturation. These findings support the continuous intravenous infusion approach to deliver uninterrupted therapeutic pressure by maintaining AMG 211 exposure of the tumor (2, 10). In addition, the absence of tumor lesion visualization might be indicative of tumor target saturation. Although an approximately 10% to 25% reduced uptake in tumor lesions after treatment has been shown via serial PET imaging for two membrane receptors targeting antibody tracers, clear evidence of tumor saturation was not found in these studies (30, 32). Also, other factors like perfusion and anatomical location could be responsible for lack of tumor visualization we observed in patients imaged during AMG 211 treatment. We observed ADAs in both patients in whom imaging during AMG 211 treatment was performed. Previously, in a phase I study, ADAs were present in 48% of patients who received AMG 211 treatment on days 1 to 5 in 28-day cycles (10), despite the fact that BiTE antibody constructs are thought to be less immunogenic due to the lack of an Fc domain in comparison with full-length antibodies (41). AMG 211 comprises a humanized CEA arm and a deimmunized CD3 arm, therefore mouse residues remain, which may be one cause for ADA generation in the absence of an Fc domain. The presence of ADAs might have altered ^{89}Zr-AMG 211 pharmacokinetics and could have led to reduced ^{89}Zr-AMG 211 availability in the blood pool by triggering an additional clearance pathway through immune complex formation and subsequent degradation through phagocytic cells in the liver and spleen (42).

In this study, we demonstrated that imaging with ^{89}Zr-AMG 211 is very informative regarding CEA/CD3 BiTE antibody construct, whole-body biodistribution, and tumor targeting. We showed CD3-specific tracer accumulation in lymphoid organs and clear tumor uptake that was highly heterogeneous, both within and between patients. This approach can support rational trial design for such innovative antibody targeting strategies.

Disclosure of Potential Conflicts of Interest

E.G.E. de Vries is a consultant/advisory board member for Sanofi, Daiichi Sankyo, NSABP, Pfizer, and Merck. No potential conflicts of interest were disclosed by the other authors.

Authors' Contributions

Conception and design: K.L. Moek, F.V. Suurs, J.A. Gietema, M.N. Lub-de Hooge, R.S.N. Fehrmann, E.G.E. de Vries
Development of methodology: K.L. Moek, S.J.H. Waaijer, C.P. Schröder, M.N. Lub-de Hooge
Acquisition of data (provided animals, acquired and managed patients, provided facilities, etc.): K.L. Moek, S.J.H. Waaijer, I.C. Kok, A.H. Brouwers, C.W. Menke-van der Houven van Oordt, C.P. Schröder, A. Jorritsma-Smit, M.N. Lub-de Hooge, R.S.N. Fehrmann, D.J.A. de Groot, E.G.E. de Vries
Analysis and interpretation of data (e.g., statistical analysis, biostatistics, computational analysis): K.L. Moek, S.J.H. Waaijer, I.C. Kok, A.H. Brouwers, C.W. Menke-van der Houven van Oordt, C.P. Schröder, S.V.K. Mahesh, R.S.N. Fehrmann, D.J.A. de Groot, E.G.E. de Vries
Writing, review, and/or revision of the manuscript: K.L. Moek, S.J.H. Waaijer, I.C. Kok, F.V. Suurs, A.H. Brouwers, C.W. Menke-van der Houven van Oordt, T.T. Wind, J.A. Gietema, C.P. Schröder, A. Jorritsma-Smit, M.N. Lub-de Hooge, R.S.N. Fehrmann, D.J.A. de Groot, E.G.E. de Vries
Administrative, technical, or material support (i.e., reporting or organizing data, constructing databases): K.L. Moek, T.T. Wind, M.N. Lub-de Hooge, D.J.A. de Groot
Study supervision: R.S.N. Fehrmann, D.J.A. de Groot, E.G.E. de Vries

Acknowledgments

We thank the patients for participating in the study. We thank Sabine Stienen from Amgen Research Munich GmbH, and Kam Cheung from Amgen Thousand Oaks for their advice on trial design and interpretation of data. We thank Anouk Funke for her assistance in figure design. We thank Linda Pot for the labeling procedures, and Johan Wiegers and Cemile Karga for their assistance with PET data transfer. Research support from Amgen was made available to the institution. The study drug was supplied by Amgen.

The costs of publication of this article were defrayed in part by the payment of page charges. This article must therefore be hereby marked *advertisement* in accordance with 18 U.S.C. Section 1734 solely to indicate this fact.

Received September 4, 2018; revised October 28, 2018; accepted February 6, 2019; published first February 11, 2019.

References

1. Carter PJ, Lazar GA. Next generation antibody drugs: pursuit of the `high-hanging fruit'. Nat Rev Drug Discov 2018;17:197–223.
2. Klinger M, Benjamin J, Kischel R, Stienen S, Zugmaier G. Harnessing T cells to fight cancer with BiTE® antibody constructs – past developments and future directions. Immunol Rev 2016;270:193–208.
3. Kantarjian H, Stein A, Gokbuget N, Fielding AK, Schuh AC, Ribera JM, et al. Blinatumomab versus chemotherapy for advanced acute lymphoblastic leukemia. N Engl J Med 2017;376:836–47.
4. Zhu M, Wu B, Brandl C, Johnson J, Wolf A, Chow A, et al. Blinatumomab, a bispecific T cell engager (BiTE(®)) for CD-19 targeted cancer immunotherapy: clinical pharmacology and its implications. Clin Pharmacokinet 2016;55:1271–88.
5. Goebeler ME, Knop S, Viardot A, Kufer P, Topp MS, Einsele H, et al. Bispecific T cell engager (BiTE) antibody construct blinatumomab for the treatment of patients with relapsed/refractory non Hodgkin lymphoma: final results from a phase I study. J Clin Oncol 2016;34:1104–11.
6. Blumenthal RD, Leon E, Hansen HJ, Goldenberg DM. Expression patterns of CEACAM5 and CEACAM6 in primary and metastatic cancers. BMC Cancer 2007;7:2.
7. Hammarström S. The carcinoembryonic antigen (CEA) family: structures, suggested functions and expression in normal and malignant tissues. Semin Cancer Biol 1999;9:67–81.
8. Osada T, Hsu D, Hammond S, Hobeika A, Devi G, Clay TM, et al. Metastatic colorectal cancer cells from patients previously treated with chemotherapy are sensitive to T-cell killing mediated by CEA/CD3-bispecific T-cell-engaging BiTE antibody. Br J Cancer 2010;102:124–33.
9. Lutterbuese R, Raum T, Kischel R, Lutterbuese P, Schlereth B, Schaller E, et al. Potent control of tumor growth by CEA/CD3-bispecific single-chain antibody-constructs that are not competitively inhibited by soluble CEA. J Immunother 2009;32:341–52.
10. Pishvaian M, Morse MA, McDevitt J, Norton JD, Ren S, Robbie GJ, et al. Phase 1 dose escalation study of MEDI-565, a bispecific T-cell engager that targets human carcinoembryonic antigen, in patients with advanced gastrointestinal adenocarcinomas. Clin Colorectal Cancer 2016;15:345–51.
11. Moek KL, Fiedler W, von Einem JC, Verheul H, Seufferlein T, de Groot DJ, et al. Phase I study of AMG 211/MEDI-565 administered as continuous intravenous infusion for relapsed/refractory gastrointestinal (GI) adenocarcinoma [abstract]. In: Proceedings of the ESMO 2018 Congress; 2018 Oct 22; Munich, Germany. Lugano, (Switzerland): ESMO; 2018; Abstract nr 427P.
12. Tibben JG, Boerman OC, Massuger LFAG, Schijf CP, Claessens RA, Corstens FH. Pharmacokinetics, biodistribution and biological effects of intravenously administered bispecific monoclonal antibody OC/TR F(ab')2 in ovarian carcinoma patients. Int J Cancer 1996;66:477–83.
13. Menke-van der Houven van Oordt CW, van Brummelen E, Nayak T, Huisman M, de Wit-van der Veen L, Mulder E, et al. 89Zr-labeled CEA-targeted IL-2 variant immunocytokine in patients with solid tumors: CEA mediated tumor accumulation in a dose-dependent manner and role of IL-2 receptor-binding. Ann Oncol 2016;27:358O.
14. Waaijer SJH, Warnders FJ, Stienen SK, Friedrich M, Sternjack A, Cheung HK, et al. Molecular imaging of radiolabeled bispecific T-cell engager 89Zr-AMG211 targeting CEA-positive tumors. Clin Cancer Res 2018;24: 4988–96.
15. Wolchok JD, Hoos A, O'Day S, Weber JS, Hamid O, Lebbé C, et al. Guidelines for the evaluation of immune therapy activity in solid tumors: immune-related response criteria. Clin Cancer Res 2009;15:7412–20.
16. Verel I, Visser GW, Boellaard R, Stigter-van Walsum M, Snow GB, van Dongen GA. 89Zr immuno-PET: comprehensive procedures for the production of 89Zr-labeled monoclonal antibodies. J Nucl Med 2003;44: 1271–81.
17. National Cancer Institute, Common terminology criteria for adverse events v4.0; 2009 Available from: https://www.eortc.be/services/doc/ctc/CTCAE_4.03_2010-06-14_QuickReference_5x7.pdf.
18. Makris NE, Boellaard R, Visser EP, de Jong JR, Vanderlinden B, Wierts R, et al. Multicenter harmonization of 89Zr PET/CT performance. J Nucl Med 2014;55,264–7.
19. Loening AM, Gambhir SS. AMIDE: a free software tool for multimodality medical image analysis. Mol Imaging 2003;2:131–7.
20. Molina DK, DiMaio VJ. Normal organ weights in women: part II – the brain, lungs, liver, spleen, and kidneys. Am J Forensic Med Pathol 2015;36: 182–7.
21. Molina DK, DiMaio VJ. Normal organ weights in men: part II – the brain, lungs, liver, spleen, and kidneys. Am J Forensic Med Pathol 2012;33: 368–72.
22. Deurenberg P, Weststrate JA, Seidell JC. Body mass index as a measure of body fatness: age- and sex-specific prediction formulas. Br J Nutr 1991;65: 105–14.
23. Nadler SB, Hidalgo JH, Bloch T. Prediction of blood volume in normal human adults. Surgery 1962;51:224–32.
24. Brinkmann U, Kontermann RE. The making of bispecific antibodies. MAbs 2017;9:182–212.
25. Mandikian D, Takahashi N, Lo AA, Li J, Eastham-Anderson J, Slaga D, et al. Relative target affinities of T-cell dependent bispecific antibodies determine biodistribution in a solid tumor mouse model. Mol Cancer Ther 2018;17: 776–85.
26. Leong SR, Sukumaran S, Hristopoulos M, Totpal K, Stainton S, Lu E, et al. An anti-CD3/anti-CLL-1 bispecific antibody for the treatment of acute myeloid leukemia. Blood 2017;129:609–18.
27. Lehmann S, Perera R, Grimm HP, Sam J, Colombetti S, Fauti T, et al. In vivo fluorescence imaging of the activity of CEA TCB, a novel T-cell bispecific antibody, reveals highly specific tumor targeting and fast induction of T-cell-mediated tumor killing. Clin Cancer Res 2016;22:4417–27.
28. Oberst MD, Fuhrmann S, Mulgrew K, Amann M, Cheng L, Lutterbuese P, et al. CEA/CD3 bispecific antibody MEDI-565/AMG 211 activation of T cells and subsequent killing of human tumors is independent of mutations commonly found in colorectal adenocarcinomas. MAbs 2014;6:1571–84.
29. Chetty R, Gatter K. CD3: structure, function, and role of immunostaining in clinical practice. J Pathol 1994;173:303–7.
30. Oosting SF, Brouwers AH, van Es SC, Nagengast WB, Oude Munnink TH, Lub-de Hooge MN, et al. 89Zr-bevacizumab PET visualizes heterogeneous tracer accumulation in tumor lesions of renal cell carcinoma patients and differential effects of antiangiogenic treatment. J Nucl Med 2015;56:63–9.
31. Lamberts LE, Menke-van der Houven van Oordt CW, ter Weele EJ, Bensch F, Smeenk MM, Voortman J, et al. ImmunoPET with anti-mesothelin antibody in patients with pancreatic and ovarian cancer before anti-mesothelin antibody-drug conjugate treatment. Clin Cancer Res 2016;22:1642–52.
32. Bensch F, Lamberts LE, Smeenk MM, Jorritsma-Smit A, Lub-de Hooge MN, Terwisscha van Scheltinga AGT, et al. 89Zr-lumretuzumab PET imaging before and during HER3 antibody lumretuzumab treatment in patients with solid tumors. Clin Cancer Res 2017;23:6128–37.
33. Baban DF, Seymour LW. Control of tumour vascular permeability. Adv Drug Deliv Rev 1998;34:109–19.
34. Keyaerts M, Xavier C, Heemskerk J, Devoogdt N, Everaert H, Ackaert C, et al. Phase I study of 68Ga-HER2-nanobody for PET/CT assessment of HER2 expression in breast carcinoma. J Nucl Med 2016;57:27–33.
35. Vaneycken I, D'huyvetter M, Hermot S, de Vos J, Xavier C, Devoogdt N, et al. Immuno-imaging using nanobodies. Curr Opin Biotechnol 2011;22: 877–81.

Published OnlineFirst February 11, 2019; DOI: 10.1158/1078-0432.CCR-18-2918

36. Beylergil V, Morris PG, Smith-Jones PM, Modi S, Solit D, Hudis CA, et al. Pilot study of 68Ga-DOTA-F(ab')2-trastuzumab in patients with breast cancer. Nucl Med Commun 2013;34:1157–65.
37. Dijkers EC, Oude Munnink TH, Kosterink JG, Brouwers AH, Jager PL, de Jong JR, et al. Biodistribution of 89Zr-trastuzumab and PET imaging of HER2-positive lesions in patients with metastatic breast cancer. Clin Pharmacol Ther 2010;87:586–92.
38. Wittrup KD, Thurber GM, Schmidt MM, Rhoden JJ. Practical theoretic guidance for the design of tumor-targeting agents. Meth Enzymol 2012; 503:255–68.
39. Arvedson TL, Balazs M, Bogner P, Black K, Graham K, Henn A, et al. Generation of half-life extended anti-CD33 BiTE® antibody constructs compatible with once-weekly dosing [abstract]. In: Proceedings of the American Association for Cancer Research Annual Meeting 2017; 2017 Apr 1–5; Washington, DC. Philadelphia (PA): AACR; Cancer Res 2017; Abstract nr 55.
40. Lorenczewski G, Friedrich M, Kischel R, Dahlhoff C, Anlahr J, Balaz M, et al. Generation of a half-life extended anti-CD19 BiTE antibody construct compatible with once-weekly dosing for treatment of CD19-positive malignancies. Blood 2017;130:2815.
41. Rathi C, Meibohm B. Clinical pharmacology of bispecific antibody constructs. J Clin Pharmacol 2015;55:S21–8.
42. Chirmule N, Jawa V, Meibohm B. Immunogenicity to therapeutic proteins: impact on PK/PD and efficacy. AAPS J 2012;14:296–302.

Published OnlineFirst February 11, 2019; DOI: 10.1158/1078-0432.CCR-18-2918

American Association for Cancer Research

Clinical Cancer Research

^{89}Zr-labeled Bispecific T-cell Engager AMG 211 PET Shows AMG 211 Accumulation in CD3-rich Tissues and Clear, Heterogeneous Tumor Uptake

Kirsten L. Moek, Stijn J.H. Waaijer, Iris C. Kok, et al.

Clin Cancer Res 2019;25:3517-3527. Published OnlineFirst February 11, 2019.